Peer-reviewed version available at Micromachines 2018, 9, 263; doi:10.3390/mi9060263

Review

Novel nano-materials and nano-fabrication techniques for flexible electronic systems

Kyowon Kang [1†], Young Uk Cho [1†] and Ki Jun Yu [1,*]

[1] Affiliation 1; School of Electrical Engineering, Yonsei University, Seoul 03722, Republic of Korea
* Correspondence: kijunyu@yonsei.ac.kr; Tel.: +82-2-2123-2769
† These authors contributed equally to this work.

Abstract: Recent progress in the fabricating flexible electronics has been developed significantly due to the increased interest of the flexible electronics which can be applied to enormous fields not only to conventional electronic devices but to bio/eco electronic devices. Flexible electronics can be applied to wide range of fields such as flexible display, flexible power storage, flexible solar cells, wearable electronics and healthcare monitoring devices. Recently, flexible electronics are being attached on the skin and even implanted into human body to monitor the bio-signals and for treatment purpose. To improve the electrical characteristic and the mechanical properties of flexible electronics, nanoscale fabrications using novel nano-materials are required. Advanced in nanoscale fabrication methods allow construction of the active materials that can combine with the ultra-thin soft substrate to form flexible electronics with high performances and reliability. In this review, wide range of nanoscale fabrication methods for flexible electronics classified in either top-down or bottom-up approaches such as conventional photolithography, soft lithography, nanoimprint lithography, growth, assembly and chemical vapor deposition(CVD) will be reported with specific fabrication processes and results. Here, our aim is to introduce various fabrication methods that can be used to fabricate the flexible electronics.

Keywords: flexible electronics; nano-fabrication; top-down approaches; bottom-up approaches

1. Introduction

Nowadays, standard electronic devices require multi-functional platforms in limited substrate area. To keep in pace with demands for device users, nanofabrication process for flexible electronics[1-5] is deeply studied in a variety of field such as multi-functional energy storage devices[6-8], wearable devices for human healthcare[9-12], and displays[13-15] with great practicality and reliability.

More specifically, approaches to the device fabrication with mechanical flexibility can be divided into two dominant processes; top-down[16-19] and bottom-up[20-22] approaches. The main difference between the top-down and the bottom-up approach is a mechanisms and methods for the initial state, such as from bulk-structure to the desired flexible device for top-down or the completely opposite method for bottom-up. Here, we introduce ultrathin nano-material structures and fabrication methods that allow assemblies of heterogeneous integration of functional materials onto soft substrates, with all the active components to maintain excellent electronic functions. The flexible and stretchable electronic systems with performance that reaches or exceed the levels comparable to those of conventional electronic systems are classified. This review summarizes some recent progress in the field of micro- and nano-electronics, and shows the novel electronic devices for the practical applications.

Peer-reviewed version available at Micromachines 2018, 9, 263; doi:10.3390/mi9060263

2. Novel Devices Designed by Top-down Nanofabrication

Top-down approach is the process that the structure is cut out from the bigger thing. Specially, in the area of macro-electronics, top-down approach would be more desirable because various materials can be produced by conventional lithographic process[23,24] and etching techniques[25-27]. The lateral dimensions of this method can range from tens of nanometer to the mm scales. Also, freestanding single-crystal sheet type can be created from wafers by employing an embedded release layer to yield flexible systems. Thus, nanostructures are synthesized by etching the layers on the substrate. However, it is impossible to conduct the entire process on the flexible substrate, such as doping process and chemical vapor deposition(CVD) because these processes require high temperatures that significantly deform the flexible substrates[28]. To resolve this issue, transfer-printing process and a method of releasing from the rigid substrate are integrated to form flexible electronics[29-36]. Here, various flexible electronic devices fabricated using top-down approach are introduced in the following contents.

First, photonic and plasmonic flexible devices based on eco-friendly hydroxypropyl cellulose(HPC) are introduced in Figure 1a[37]. In general, when the nanoscale celluloses exist in the form of fibers, they may not be seen white color, but has a transparent or iridescent property. This optical property can be arbitrarily adjusted by the structure of the particles either the amorphous state or the single-crystalline state. Using a special chiral behavior[38-41] possessed by the HPC solution, simple nanostructured design provides enhanced photoluminescence and potential of the HPC plasmonic membrane as a role of optical device. Core fabrication process is focused on exploiting soft lithography[42-46] rather than using conventional photolithography or growth method. Soft lithography realizes the cost-effective process with patterning large area, ensuring enhanced reproducibility. Figure 1b shows two specific approaches to fabricate photonic HPC films. First one is the hot-embossing process. Spin-casted HPC on the rigid substrate is heated, followed by a hard polydimethylsiloxane(h-PDMS) compound-based patterning. And then the HPC photonic film is transferred onto the flexible substrate to complete the device fabrication. Second method is to use a replica molding process. On the surface of a h-PDMS mold, HPC solution is poured and dried by applying heat. Finally, free-standing, flexible photonic HPC film is obtained by peeling off from the PDMS mold. The entire structures acquired from both methods are almost identical, but hot-embossing process presented better optical property. After depositing and patterning metal on the HPC photonic films, the fabrication of HPC films can be completed. Figure 1c shows the scanning electron microscope(SEM) image of plasmonic HPC film patterned with arrays of hexagonal lattice structure. This unique nanostructure upgrades the photoluminescence, by maintaining its iridescent property with amplified optical extinction spectra.

The flexible electronics fabricated by top-down approaches can be directly applied to medical application due to the absence of mechanical mismatch between the flexible electronics and organs or tissues of human body. The contents to be introduced next are new bio-integrated devices that can be widely applied in medical treatment/diagnosis. Here, we introduce the devices that can be formed by lifting off a thin layer from a temporary substrate using chemical dissolution[47,48], then transfer-printing completed electronic systems from a rigid substrate to a flexible substrate.

In the first instance, to distinguish the normal tissue from the abnormal one, highly flexible microscale piezoelectric device is developed[49]. Exploiting alteration of mechanical properties of tissue modulus in accordance with lesions expression[50-54], minimally invasive novel probe offers quantitative agreement with clinical insights. Exploded schematic views of the specific structures are shown in Figure 1d. The thin, photolithographically patterned and defined triple layer membrane, composed of Au/Cr, piezoelectric material lead zirconate titanate(PZT), and Ti/Pt materials, is used both as an actuator and a sensor simultaneously. Each of the components is transfer-printed onto the PI substrate from the donor wafer regardless of the structure in the form of either the free-standing device or the integration on a biopsy needle. After encapsulating the triple layer with PI, another layer of PI is encapsulated after the interconnecting Au lines. Figure 1e shows the images of the freestanding probe placed onto biological tissue environment and wrapped the device around the surface of the conventional biopsy needle. The bottom right magnified image in Figure 1e designates

the point of actuator/sensor region on the needle. Fundamental device operation is followed based

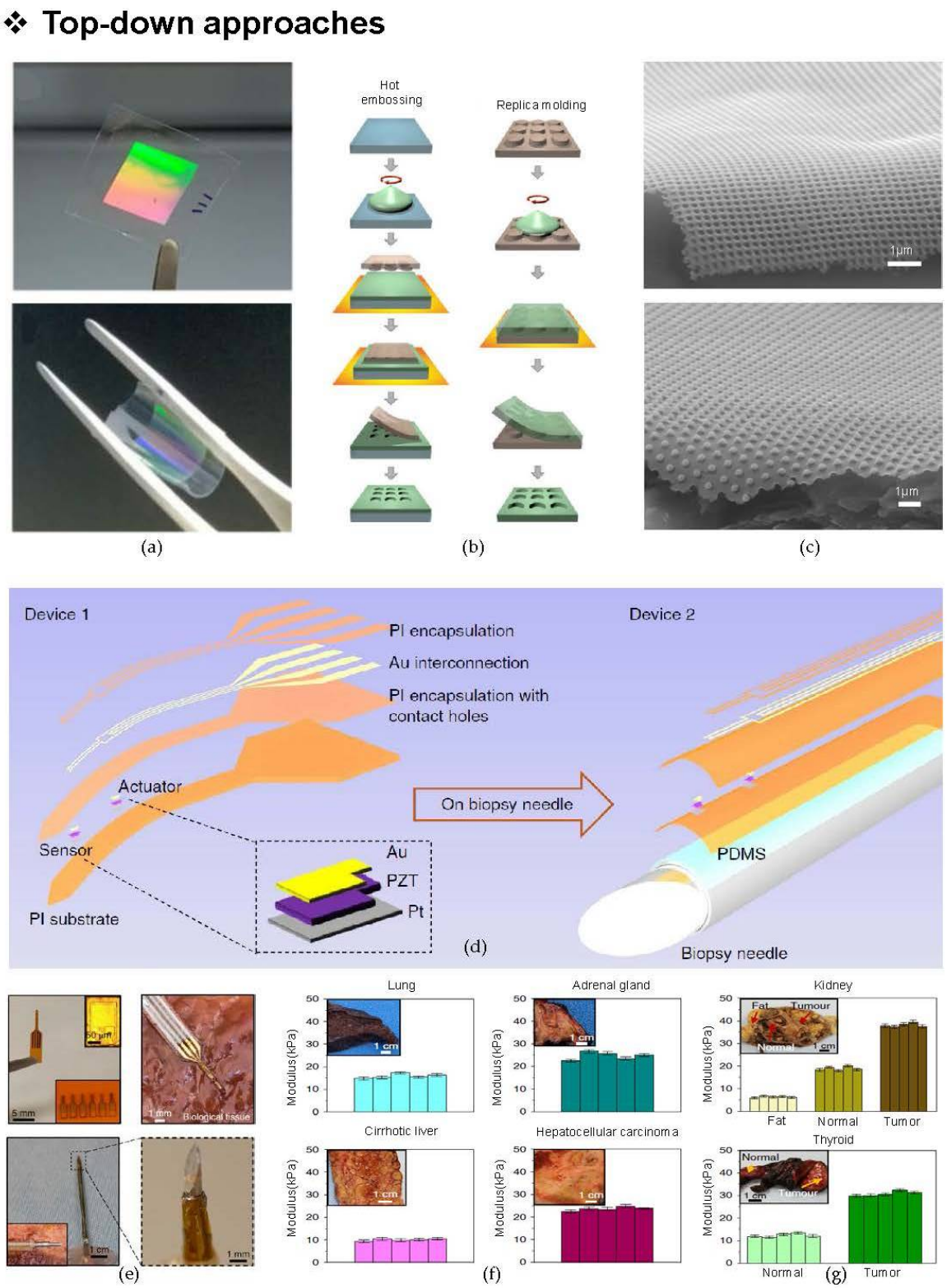

Figure 1. HPC photonic thin film with hexagonal nanopillar structure / Flexible, piezoelectric tissue modulus recording probes (**a**) An image of HPC photonic crystal(top) and mechanical flexibility with a free-standing property of the design(bottom); (**b**) Schematics of two fabrication processes to make HPC photonic films-Hot embossing and Replica molding methods. The blue-colored slide indicates glass substrate, green one for HPC, brown one for hard PDMS, respectively; (**c**) Special hexagonal nanopillar images by SEM lateral view. Paper substrates are used to imprint predesigned nanopattern. Copyright 2018 Nature; (**d**) Illustrations of two main PZT based modulus probes; free-standing device(left) and conformally attached device on a biopsy needle(right); (**e**)

Pictures of self-standing devices(top) and the device on the biopsy needle(bottom). Inset picture (top, upper-right) designates a pair of sensor/actuator and the other inset picture (top, down-right) shows a row of completed designs. Magnified picture(bottom) shows specific actuator/sensor sites; (**f, g**) Results of measured modulus of human tissues in a variety of organs with PZT based probe. Inset pictures of the upper-left side of the respective graphs show optical images of organs in which modulus sensing conducted. Copyright 2018 Nature

on the piezoelectric effect[55-59]. When the device achieves conformal contact with tissue interface, induced potential makes piezoelectric strain at the actuator. The tissue which has a part of deformation transfers this force to the sensor, and then some strain force is changed into a certain value of voltage, thereby making measurement of tissue modulus be realized. Figure 1f shows the results of tissue modulus conducted in human organs such as fresh lung, adrenal gland, fresh cirrhotic liver, and hepatocellular carcinoma. As estimated, Figure 1f provides information that cirrhotic liver maintains average modulus about 10kPa, while the cancerous hepatocellular tissue makes peak modulus about 23kPa. Modulus Graph in Figure 1g also shows different values of modulus between the fresh tissue part and the abnormal tissue site from the human thyroid and formalin-treated kidney. In this work, devices offer an underwork for the modulus-measuring platforms for biopsy guidance, based on magnetic resonance elastography[60-64].

Top-down approach for nanopatterning can be also extensively applied to electrophysiology mapping[65-68] or electrical/optical stimulating systems[69-75]. Recently, opto-genetics is extensively studied, because of its delicate controllability of neural activity by selectively modifying channel-rhodopsin treated genes with light. Entirely seamless implantable optoelectronic device that let axons react directly in accordance with light stimulating is introduced in Figure 2a[76]. The RF harvesting unit rectifies the signals that received from the transmitter and routes the output current for the optical energy(LED). And then, interconnected serpentine-structured Ti/Au antenna layer diminishes the resonant frequency with maintaining wide bandwidth requisite for the efficient energy harvest at certain frequency. Fabrication process for the device is initiated from the spin-casting of polyimide(PI) onto the polymethyl methacrylate(PMMA) coated on glass surface. And then, the bilayers of Ti/Au are deposited by the e-beam evaporator and photolithographically patterned in serpentine structure to form an antenna. After the encapsulating the completed device with polydimethylsiloxane(PDMS), this component is immersed in acetone solution to dissolve the PMMA layer. Finally, thin free-standing composite optogenetic device is released from the glass, featuring soft, flexible property. This flexible, stretchable state optimizes conformal contact between the surface of the tissue and device. Optogenetic controlling experiment is conducted mainly into two parts; underneath gluteus maximus muscle and epidural space in the lumbar spinal cord of mice, as shown in Figure 2b and 2c. To determine the device functionality as an optogenetic platform, an experiment of Ch R2 activation for nociceptive reaction of mice with spontaneous pain expression, following space abhorrence is conducted. Figure 2d and 2e demonstrates the nociceptive pathways and LED stimulating formation of the device that is fully implanted at sciatic nerve and epidural space in the Ch R2 expressive mice, respectively. Rotarod test is conducted to identify either the motor activity of the experimental rodent affects the performance of the LED stimulator (Figure 2i). The result provides the fact that there is no changing balance of the device. For specific experimental data, both mice expressing Ch R2 and control units are introduced to the y-shaped maze, where mice can arbitrarily move to both sides of the maze pathways. Especially, at the left side of the passage in y-shaped maze, there is a RF antenna which makes the implanted LED be turned on, as illustrated in Figure 2h. Figure 2f and 2g show the result of the number of nociceptive expression and trend of space abhorrence checking times of staying by the Advillin-Ch R2 for sciatic nerve-implanted mice, SNS-Ch R2 for epidural space in the spinal cord of mice and control units according to the LED illumination. This result shows the correspondence of expected simulation, presenting the potential for the clinical devices as a novel optogenetic therapy system[77,78] with great advantages such as physical tether-free and external feature free characteristics.

Preprints (www.preprints.org) | NOT PEER-REVIEWED | Posted: 2 May 2018 doi:10.20944/preprints201805.0027.v1

Peer-reviewed version available at Micromachines 2018, 9, 263; doi:10.3390/mi9060263

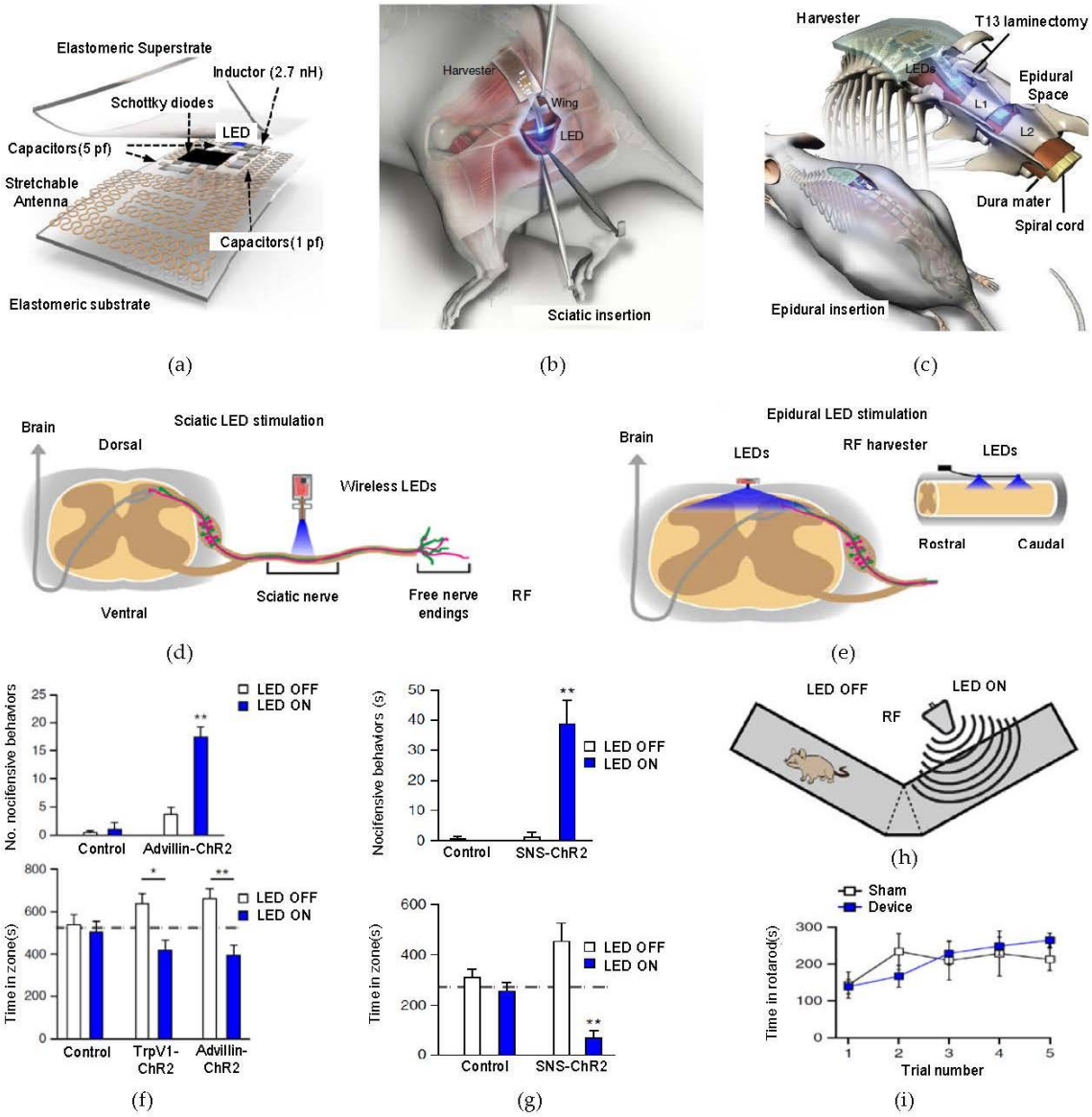

Figure 2. Fully implantable, flexible systems for wireless optogenetic stimulator with related experiments. (**a**) Schematics of fully implantable, flexible electronic systems for wireless optogenetic stimulator; (**b**) Sciatic insertion surgery to implant the completed device into the spinal cord. Wing-shaped LED extension site pass from the gluteus maximus to the sciatic nerves; (**c**) Similar implantation is conducted at the epidural space in the spinal cord; (**d, e**) Illustration of nociception path with a LED stimulator in a sciatic nerve and epidural space, respectively; (**f, g**) Graphs of numbers of adverse behaviors/Time in y-maze observed by the rodents treated Advillin-ChR2 in accordance with the LED stimulation in the sciatic nerve and epidural space, respectively; (**h**) Experimental y-maze illustration. Using RF signal, pathways are separated by LED ON/OFF environments; (**i**) Graph of a rotarod performance result. This graph shows motor activity does not change the entire performance of the device. Copyright 2015 Nature

The method of releasing an active device from rigid substrates to obtain a mechanical flexibility of the device is efficiently used in multifunctional cardiac patches (Figure 3a)[79]. These novel cardiac patches are composed of three main parts; electronic system for sensing & stimulating, electroactive polymer-deposited electrode sites for chemical factor diffusion for controlling cell function, and three-dimensional(3D) dense nanofiber scaffolds in the cardiac cell environment. A detailed fabrication process is illustrated in Figure 3b. The device fabrication begins with depositing nickel as a relief layer onto the silicon substrate. And then, the spin-casting and curing of SU-8 photoresist on the surface of the Ni layer followed by the Cr/Au metal lift-off process. Subsequently, titanium

nitride(TiN) layer is deposited on the gold pads by sputtering to increase their surface area. Passivated components of the design are released from the previous silicon substrate and remains free-standing, flexible structure by etching the Ni relief layer using nitric acid. Figure 3c is an image of flexible device which consists of 32 electrodes with SU-8 mesh structure.

Fascinating cardiac cell cultures are optimized by the stitched structure-like nanofiber based biomaterial scaffolds. As shown in Figure 3d, an integration of the biomaterials gives a potential for on-demand drug release to control the tissue functions without interfering cardiac cells with seeding. Schematic representation and picture of device cultivated in the cardiac site in Figure 3e indicate the process for the cell culture and its foldable scaffold structure with the reliable cell viability. Electrical signals recording acquired by cardiomyocytes is done from nine gold electrodes in the device shown in Figure 3f. As a result, all nine electrodes showed the similar results as the signal generated by cardiomyocyte. Figure 3g presents the result of cardiac patch sensing for the signal frequency twice as high as that of administering norepinephrine and the integrated quantification recording through calcium imaging.

In addition to the ability to sense temporarily electrophysiological signals from the brain, a multiplexed bio-resorbable arrays of the silicon transistor are introduced in Figure 3h[80]. This particular device is implanted over a cortical surface of a rat brain and functions programmed time period and resorbs in the body of the rat. Because the device only consists of biocompatible and biodegradable materials, the secondary surgery to extract the device is not required. After recording brain activities for predefined periods of time, but the device gradually dissolves in the body. The device is based on the actively multiplexed array with Si nano-membrane (SiNM) NMOS transistors, which serve as the sites of the electrode. SiO_2 layer and Mo serve as a gate insulator and contacts for the source, drain, and gate, respectively. Two sets of triple layers of $SiO_2/Si_3N_4/SiO_2$ provide interlayer dielectric and encapsulation barriers. Fabrication begins with the silicon on insulator(SOI) wafer which is doped with phosphorous sources to form source and drain for NMOS transistors. And then, the Si NM layer is separated from the bulk Si wafer by dissolving a box SiO_2 layer using hydrofluoric acid(HF). SiNM is then transfer-printed onto a diluted PI/PMMA/Si substrate using PDMS stamp, followed by isolating of SiNM, depositing SiO_2 as a gate dielectric and MO for source, drain and gate contacts to form the active matrix. The device is encapsulated and isolated with trilayers of $SiO_2/Si_3N_4/SiO_2$. Also, another layer of MO deposited on via holes separates the columns and rows interconnects. Finally, encapsulating the device with another layer of diluted PI and forming mesh structures by photolithography lead to transferring the entire active layer to bio-resorbable substrate. After dissolving PMMA layer by acetone to release the entire device, the mesh is consequently transferred onto the surface of the bio-resorbable poly (lactic- co -glycolic acid) (PLGA) substrate to finalize the device fabrication. Soak testing is conducted in phosphate buffer saline (PBS, pH 7.4) solution in Figure 3i (top). Figure 3i (bottom) shows the image of a conformally implanted bio-resorbable array in the left hemisphere and the control electrode in the right hemisphere of an anaesthetized rat brain for *in vivo* recording. A series of eight movie frames from each epileptic spike activity which is induced by applying picrotoxin is shown in Figure 3j. The electrical mapping results of different forms of spikes (e.g., clockwise spiral, lower right to upper-left diagonal, upper left to lower-right diagonal, and right to left sweep) recorded from the electrodes, clearly demonstrate the spatio-temporally resolved neural propagation, thereby ensuring a potential device use in clinical area or health-care system.

Peer-reviewed version available at Micromachines 2018, 9, 263; doi:10.3390/mi9060263

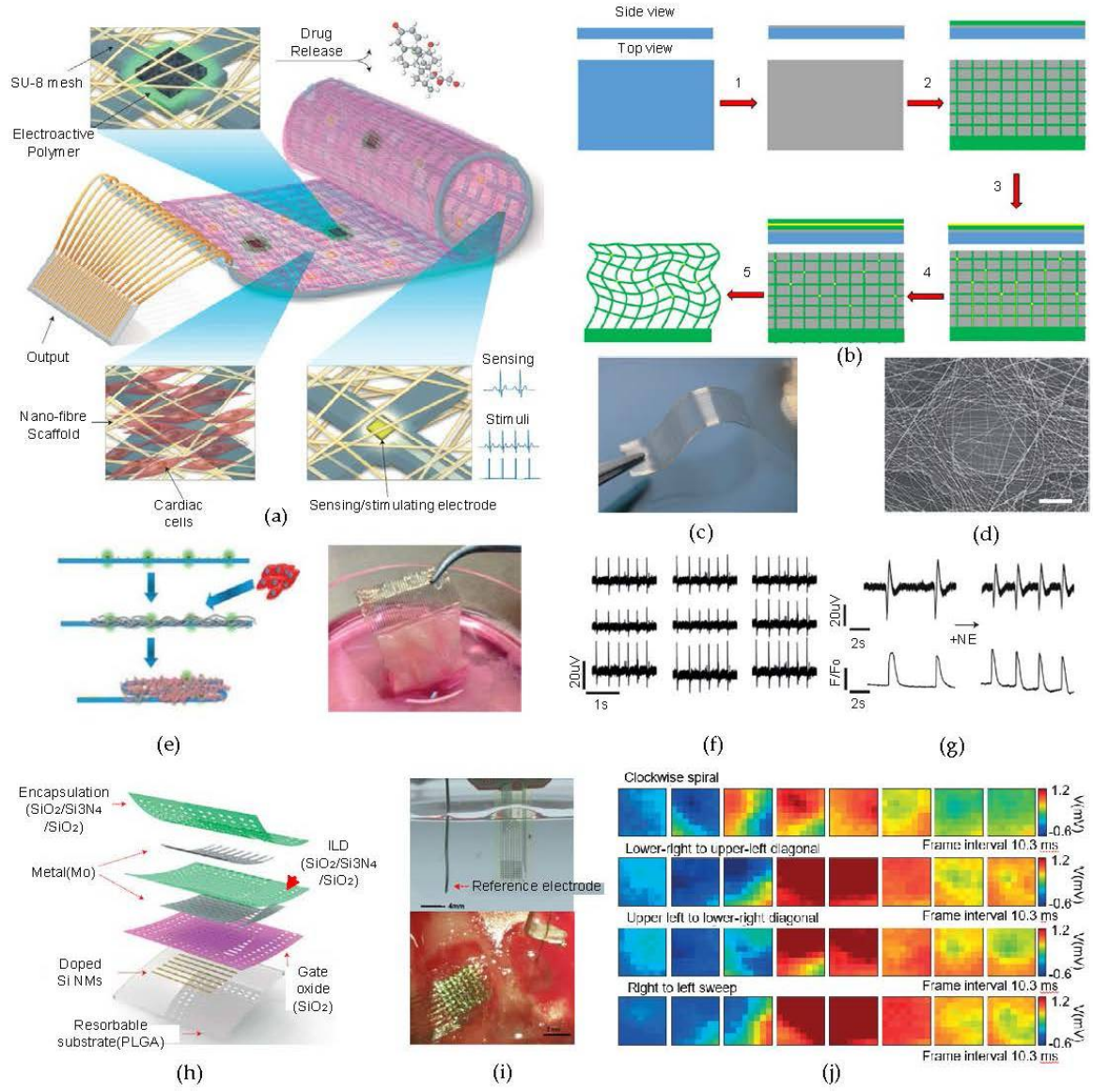

Figure 3. Multifunctional electronic system with biomaterial-based 3D scaffold cardiac patches / Multiplexed bio-resorbable silicon based design for brain mapping. (**a**) Designed cardiac patches for recording electrical tissue activity/providing electrical stimulation/spatial releasing biochemical factors; (**b**) Detailed fabrication process of cardiac patches. Upper picture is the side view and the bottom picture for the top view of the device. Components indicate temporary silicon wafer(blue), nickel layer(gray), SU-8 resist(green), and Au(yellow), respectively. 1. Deposition of 20nm nickel relief layer 2. Photolithography of SU-8 for mesh structure 3. Patterning and Cr/Au deposition followed by metal lift-off process and titanium nitride(TiN) layer deposition 4. Substrate coating with a uniform layer of SU-8 and followed by photolithography & curing 5. Releasing the device from the substrate by etching the nickel layer with nitric acid; (**c**) A picture of a flexible device comprising 32 gold electrodes with a mesh of SU8; (**d**) SEM image of larger size electrode in the cardiac patches with nanofiber-based three-dimensional scaffolds; (**e**) Schematics of foldable patches with conformal cell culture(left). Brown dots are electrodes which are used to release chemical factors. Gray serpentine lines are compounds of 3D biomaterial scaffolds, and Pink lines are seeded cardiac cells. An image of the device in cell cultures(right); (**f**) Results of electrical signals from the cardiac tissues recorded by nine gold electrodes; (**g**) Images of increased signal frequency after treating neurotransmitter(norepinephrine) on the tissue(top) and integrated recordings through calcium imaging(bottom). Copyright 2016 Nature; (**h**) An exploded schematic of compositions of actively multiplexed brain-mapping sensor based on the highly doped SiNM; (**i**) Bio-resorbable device in PBS with a reference electrode(top) and a magnified image of implanted device at the left side of the rat

hemisphere(bottom); (j) Epilepsy signal-traced brain mapping results acquired by electrode channels from the device with various spikes. Copyright 2016 Nature

3. Novel Device Designed by Bottom-up Nanofabrication

The components of the flexible electronic devices in nanoscale can be fabricated using stacking the atoms or chemicals from the bottom to the top, referred as bottom-up approaches which have distinctive advantages in some aspect compared to top-down approaches. Device fabrication process can be controlled precisely by using bottom-up approaches and can be achieved at relatively lower temperature so that there is no need to take a risk of substrate deformation due to the applied heat[81]. There are various approaches to fabricate components of the device with novel materials using bottom-up approaches such as growth method[82-86], assembly methods[87-89], and chemical vapor deposition(CVD)[90-92].

With the conventional CVD process, large-scale MoS_2 film has poor electrical properties such as low field effect mobility of lower than $15cm^2V^{-1}s^{-1}$[93-96]. On the other hand, using $MoSe_2$ as an active layer, high mobility can be achieved. To form $MoSe_2$ device layer with high field-effect mobility, modified CVD(mCVD) process which uses polycrystalline compounds of $MoSe_2$ as precursor that directly synthesized on SiO_2 is used. (Figure 4a) High mobility transistor based on crystalline $MoSe_2$ film grown on SiO_2 insulator[91] can be fabricated with field effect mobility of $121cm^2V^{-1}s^{-1}$. $MoSe_2$ film fabricated via mCVD has hexagonal shape grains whereas $MoSe_2$ film fabricated via conventional CVD process has triangular shape grains. (Figure 4b, c) Figure 4d shows the transfer curves of $MoSe_2$ transistor with different bending regimes. The black, red, and green curves represent the $MoSe_2$ TFT without bending and with the bending radius of 10mm and 5mm respectively as shown in Figure 4e. As a result, no significant changes or shifts in transfer curves are found while changing the bending radius of the device. Therefore, $MoSe_2$ TFTs fabricated by modified CVD process are endurable to induced mechanical stress while maintaining their electrical performance.

Self-assembly method is another novel nano-fabrication technique which uses specific affinity between two molecules[97-99]. Molecules that are used to form self-assembled layer have high interaction forces which are noncovalent interactions so that the monolayer can be formed tightly. Van der Waals[100,101], hydrogen bonds[102], π-π interactions[103,104] are the representing examples of noncovalent interactions used in self-assembly method. Various nano-materials can be used for self-assembly technique; from graphene to gold nanowires(AuNWs). Here, solution based self-assembled nanomesh using aged gold nanowires(AuNWs) is fabricated[89]. As Figure 4f shows, keeping the fresh AuNWs for 12 hours before drop-casting to form aged AuNWs. Aged AuNWs self-assembled into the bundles creating continuous nanomesh structure with pore size of 8-52μm. While, steric hindrance of fresh AuNWs is stronger than wire-to-wire van der Waals force which maintains ordered structure of nanomembrane, steric hindrance and van der Waals force balance is destroyed at aged AuNWs which creates bundles of AuNWs. Due to the pores in nanomesh from aged AuNWs (Figure 4g), nanomesh film is transparent while nanomembrane formed by fresh AuNWs doesn't. In addition, nanomesh fabricated by aged AuNWs is also electrically conductive with sheet resistance of $130.1\Omega^{-1}$. The AuNWs nanomesh can be transferred onto polyethylene terephthalate (PET) with a sacrificial layer of mask sheet. While, removing the sacrificial mask by peeling off using the tape or washing with ethanol, patterned AuNWs nanomesh is preserved on PET (Figure 4h). AuNWs nanomesh can be utilized as an array of pressure sensors for the flexible touch screen as shown in Figure 6i. Nanomesh film shows the similar level of pressure sensitivity compared to that of commercial products[105].

Flexible light emitting diodes(LEDs) have been studied broadly due to its wide range of applications such as flexible displays[106-108], optoelectronic system[109-111], wearable health care system[112,113], etc. In various types of nanowires, nitride nanowires have remarkably good optoelectronics properties with excellent resistance to mechanical deformation[114]. Here, flexible LEDs based on nitride nanowires are introduced[92]. Especially, fully flexible blue LEDs with core shell of InGaN/GaN nanowires grown via metalorganic chemical vapor deposition(MOCVD) has

been demonstrated in Figure 5a. The fabricated blue LEDs as shown in Figure 5c show no degradation of light brightness down to 3mm bending radius without any encapsulation while conventional flexible LEDs require encapsulation barriers to protect the LEDs. In addition, two-layer bicolor nanowire based on flexible LEDs with lighting blue and green light at the same time have been demonstrated. To fabricate the semitransparent green LED layer which is the top layer of the two-

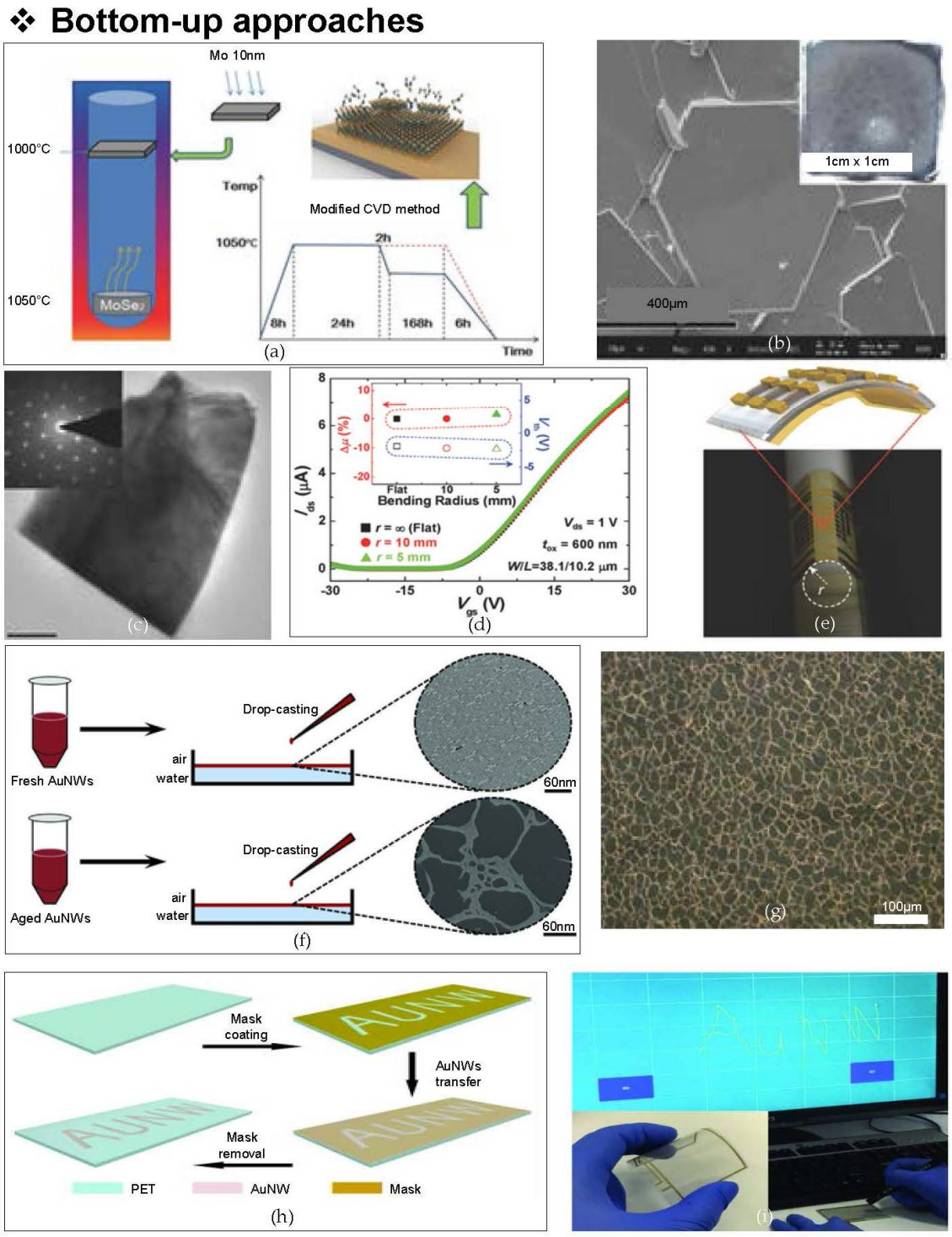

Figure 4. High-mobility transistors based on CVD-grown $MoSe_2$/Transparent and flexible nanomesh via self-assembly of ultrathin gold nanowires to fabricate flexible touch panel (**a**) Schematic of synthesis of MoSe2 film with modified CVD method; (**b**) SEM image of CVD grown MoSe2 film with hexagonal grains on Si wafer; (**c**) TEM image of dispersed MoSe2 particles and the inset image is taken from the particle via selected area electron diffraction (SAED); (**d**) I-V characteristic of unbent and bent (up to 5mm of radius) MoSe2 transistor; (**e**) Optical image of bended

Peer-reviewed version available at Micromachines 2018, 9, 263; doi:10.3390/mi9060263

MoSe2 transistor. Copyright 2016 Advanced Materials; (**F**) TEM image of AuNWs nanomembrane fabricated by fresh AuNWs solution and SEM image of AuNWs mesh film fabricated from aged AuNWs solution; (**g**) Optical image of AuNWs mesh film with pores fabricated by self-assembly method from aged AuNWs solution; (**h**) Schematic of patterning the AuNWs mesh film on the PET; (**i**) Flexible touch panel fabricated using AuNWs mesh film. Copyright 2016 Advanced Electronic Materials

layered bicolor flexible LEDs on the thin metal shell of Ni/Au, GaN nanowire arrays are embedded in PDMS and peeled off. And then, the whole layer is flipped over to deposit Ti/Au which serves as an arbitrary substrate. Since AgNWs provide high electrical conductivity, AgNWs are dispersed on the other side of deposited Ti/Au (Figure 8d 1-4)). For the fabrication of the fully transparent blue LED, fabrication process is similar to that of semitransparent LED, but instead of Ti/Au deposition, optically transparent AgNWs are dispersed on both sides of PDMS encapsulated layers (Figure 8d 5-8). The fabricated two-layer flexible LED shows no significant performance degradation of I-V characteristic or electroluminescence (EL) characteristic under 3.5 mm and 2.5 mm of bending radius with repeated bending cycles.

Nano fabrication method using bottom up approach can be utilized as smart fabrics. Nanowire strain sensor integrated with smart fabric shows good electrical characteristics[82]. Herein, wireless flexible strain sensor is applied on commercial textile via assembling hybrid carbon materials in nanoscale and piezo-resistive ZnO NWs growth on the commercial textile. This assembled hybrid carbon nanomaterials provide excellent properties in terms of robust electrical performances against a mechanical deformation due to bending. On the pristine PET textile, carbon nanotube(CNT) and reduced graphene oxide(rGO) are coated to provide excellent growth condition for ZnO nanowires[115,116]. The coated hybrid carbon nanomaterials provide the continuous conductivity and durability from the externally applied mechanical strain. Then, ZnO based texture-type strain sensor is encapsulated with thin PDMS (Figure 5e). Figure 5f, g show the current density change of bending and release of fabricated flexible textile strain sensor. The plots in Figure 5g show the flexible textile sensor monitoring the repeated bending and release of the arm up to bending angle of 60° and 120° respectively. The assembled ZnO-3 on a PET substrate textile which hybrid with carbon nanomaterials has twice higher gauge factor(GF) of 7.64 compared to that of ZnO-3 assembled on plain conventional PET film. This result implies that using the fabric-like structure as the substrate for strain sensors shows the high-pressure sensitivity and stability at the same time.

Skin-like electronics known as e-skins have been studied widely due to its wide applications such as health monitoring, medical implantation, integration of sensors, etc. Wide range of novel materials can be used to fabricate e-skins. Among those materials, graphene is one of the most widely used material to fabricate the active devices nowadays [117-120]. Graphene shows remarkable electrical conductivity, mechanical strengths, flexibility and optical transparency. With these properties of graphene and microstructured graphene layer via Layer-by-Layer (LBL) assembly method[121-124], ultra-sensitive pressure sensor can be developed. The advantages of LBL assembly method are thickness of the LBL assembled layer can be easily controlled through adjusting the number of layers and the shapes of LBL assembled layer with uniformly distributed molecules on each layer. Due to geometrical and self-limiting properties, the surface structure of the ultrathin film formed by LBL assembly method can be designed in a variety of shapes while it is not possible with other methods such as spin-coating or drop-casting[87]. Figure 6a shows the fabrication process of the ultra-sensitive flexible tactile sensor. With the KOH etched Si master mold, pyramid shapes of PDMS can be fabricated. Graphene oxide(GO) from graphite oxide suits for the LBL assembly because GO sheet has abundant negatively charges with hydroxyl and carboxyl groups. After depositing GO sheets on microstructured PDMS which improves the sensitivity via structure, GO layers were treated with hydrazine vapor to form reduced graphene oxide (rGO) which is electrically conducting graphene sheets[125,126]. rGO sheets are sandwiched between PDMS and ITO-coated PET film to construct the pressure sensor unit. The tips of pyramid shapes of rGO contacts the ITO-coated PET film which increase the sensitivity of the device. Figure 6b shows relative resistance changes ($\Delta R/R0$) of the pressure changes. The microstructured film is highly sensitive over unstructured film. Pressure response curves of the microstructured film can be subdivided into two

Peer-reviewed version available at Micromachines 2018, 9, 263; doi:10.3390/mi9060263

parts; highly sensitive at lower pressure with range of 0-100kPa and saturated sensitivity segment with range of above 100kPa. At lower pressure range(0-100kPa), pressure sensitivity slope is -5.53kPa-1 and at saturation in sensitivity range(>100kPa), pressure sensitivity slope is -0.01kPa-1 which means this highly sensitive flexible tactile sensor is ultra-sensitive at lower pressure range of 0-100kPa with ultra-fast response time of 0.2ms.

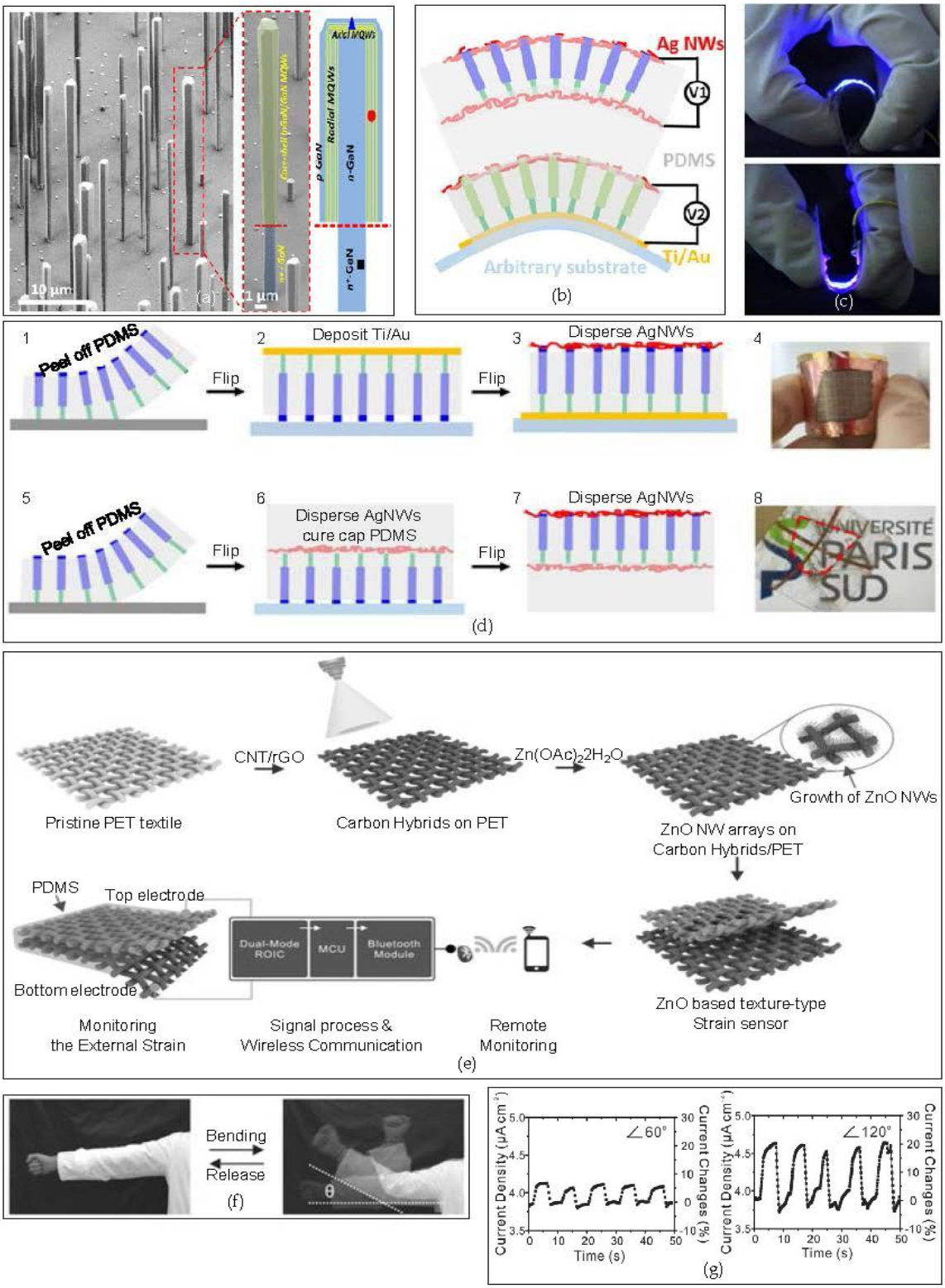

Figure 5. Flexible Light Emitting Diodes based on vertically grown nitride nanowires/Flexible textile sensor based on hybrid of carbon materials as substrate (**a**) SEM image of grown ZnO nanowire obtained with tilt angle of 45°; (**b**) Schematic of bi-layered flexible LED with blue LED for top layer and green LED for bottom layer; (**c**) Flexibility of fabricated ZnO nanowire LED; (**d**)

Schematic of fabrication process for half transparent LED (1-4) and fully transparent LED (5-8). Copyright 2015 Nano letters; (**e**) Schematic of fabricating flexible textile strain sensor fabricated via growth of ZnO nanowires; (**f, g**) Bending and releasing of the cloth made by flexible textile strain sensor and corresponding result according to the different bending angle of the arm. Copyright 2016 Advanced Functional Materials

Sensitivity can be improved via not only by structurally but also by using ultra-thin sensitive graphene film formed through self-assembly method[88]. Marangoni effect[127-129] which is the phenomenon of transferring the group due to the difference of gradient of the two differrent fluid's surface tension, was used to form ultra-thin graphene film(UGF). Figure 6d shows the schematic of how ultra-thin graphene film(UGF) is formed by self-assembly method. Graphene flakes with thickness of 2.5nm are injected on the surface of deionized(DI) water and ethanol is spread on the surface of DI water. Due to the Marangoni effect, ethanol with graphene flakes tends to move toward to high surface tension area where DI water is richer than ethanol. And then, transferred graphene flakes will collide and compacted together via π-π interactions by forming large area of UGF as shown in Figure 6e. The whole process of forming large area UGF of 150cm^2 takes only 5 seconds. The advantage of using self-assembly processes introduced here is that self-assembly process can form the uniform UGF while other methods such as drop-casting and spin-coating cannot. With UGF formed by self-assembly method, strain sensor can be fabricated. As shown in Figure 6f, UGF is transferred onto the mask which is attached on the PDMS slab. After removing mask to form 8x8 pixels, electrodes are transferred to create electronic skin with tactile sensor. UGF formed by self-assembly process show an extremely high gauge factor(GF) of 1037 at lower strain (2%). The resistance of individual graphene flakes hardly changes because of stable crystal structure. However, using the tunneling effect[130] of overlapped intersection area of self-assembled graphene flakes, the exceptionally high GF as shown in the result could be achieved. Figure 6g (top) shows the performance of the pressure sensor array, wrapped around the arm. As applied strain from the fingers, spatially resolved pressure sensing can be monitored in Figure 6g (bottom).

Monitoring the body temperature is important since numerous diseases can be characterized by the abnormal changes of body temperature. Therefore, precise and continuous temperature monitoring device is required. Recent work presents the stretchable and flexible temperature senor in the form of electronic skin with stable temperature sensing performance when external strain is applied[90]. The device consists of 5x5 SWCNT TFTs layer, two liquid metal interconnection layers and 5x5 arrays of temperature sensors layer. On the layer 1 SWCNT TFTs on PET film arrays which are fabricated via CVD process are transferred. Layer 2 and layer 3 are microchannel Ecoflex layers formed on microstructured mold. Layer 4 is temperature sensing layer with polyaniline temperature sensors on PET films. (Figure 7a, b) Four different layers were electrically connected via liquid metals which is compound form of gallium, indium, and tin. Since the device consists of the thin soft elastomer (Ecoflex), and ultrathin active components, the entire device can be stretched up to 30% of strain without device fractures or performance degradations. The completely fabricated temperature sensor can sense both heating and cooling through the normalized resistance changes with respect to the temperature changes. There is no hysteresis found on normalized resistance change for heating and cooling. Figure 7c shows, the temperature sensor arrays can be bent up to radius of 14mm maintaining its electrical performances.

In another example of e-skin, arrays of stretchable transistors are fabricated with components of polystyrene-block-poly(ethylene-ran-butylene)-block-polystyrene (SEBS) as flexible dielectric, conjugated polymer/elastomer phase separation induced elasticity (CONPHINE) film as semiconductor and spray-coated CNTs for electrodes[131]. Figure 7d shows the fabrication processes of the arrays of stretchable transistors. Rigid Si/SiO2 has been used as bottom layer to fabricate the arrays and on the top, water soluble dextran which is used as sacrificial layer to separate active layer from rigid Si/SiO2 layer has been spin-coated. Then, stretchable dielectric, stretchable semiconductor and stretchable conductor (CNT) have been patterned. SEBS is laminated on to function as flexible substrate and CNTs are patterned to form the gate electrodes. Figure 7e shows the schematic of stretchable transistor formed. The completed arrays of stretchable transistors show slight difference

Peer-reviewed version available at Micromachines 2018, 9, 263; doi:10.3390/mi9060263

of carrier mobility when applying the external stresses vertically and horizontally. (Figure 7f) The average charge-carrier mobilities from the arrays of transistor recorded 0.821±cm^{2}V^{-1}s^{-1} with highest value of 1.11 cm^{2}V^{-1}s^{-1} and on/off current ratio as 10^4 with low operation voltage of 10V. In addition,

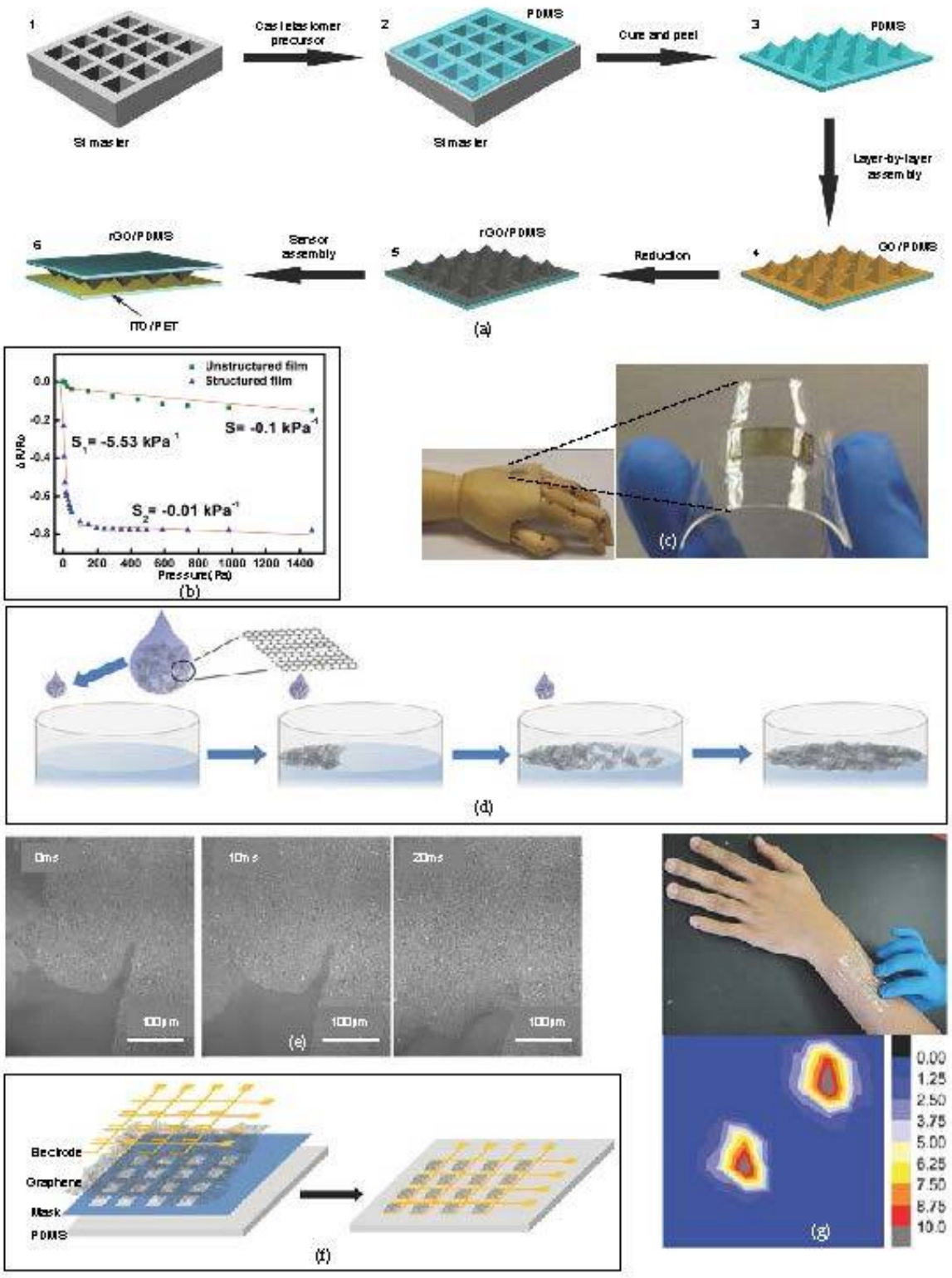

Figure 6. Microstructured graphene arrays for sensitive flexible tactile sensors/Strain sensors based on ultrathin graphene films (**a**) Schematic of fabricating flexible tactile sensor device via layer-by-layer(LBL) assembly method. Ultrathin graphene film which detects applied pressure is deposited on the PDMS film; (**b**) Pressure response curve of unstructured and structured rGO/PDMS film. The slope of relative resistance change is -5.53kPa^{-1} at range of 100Pa which shows very sensitive change at the lower pressure; (**c**) Image of tactile senor applied on the flexible substrate. Copyright 2014 Small;

(**d**) Graphene flakes forming the ultrathin graphene film(UGF) via π-π interaction of each other; (**e**) Optical image of formation of UGF in 20ms taken by high speed CCD camera; (**f**) Schematic of strain sensor fabricated from the self-assembled UGF; (**g**) Strain sensor applied on the forearm and real-time response mapping of pressure applied on the strain sensor. Copyright 2016 Advanced Materials

this stretchable transistor arrays consumes low power which suggests the potential of used as self-powered e-skins. (Figure 7f, g) Figure 7h shows the stretchable arrays of transistors attached onto the palm. The device can detect very small pressure change with high spatially resolved pattern and sensitivity even when the artificial lady bug sits on the device.

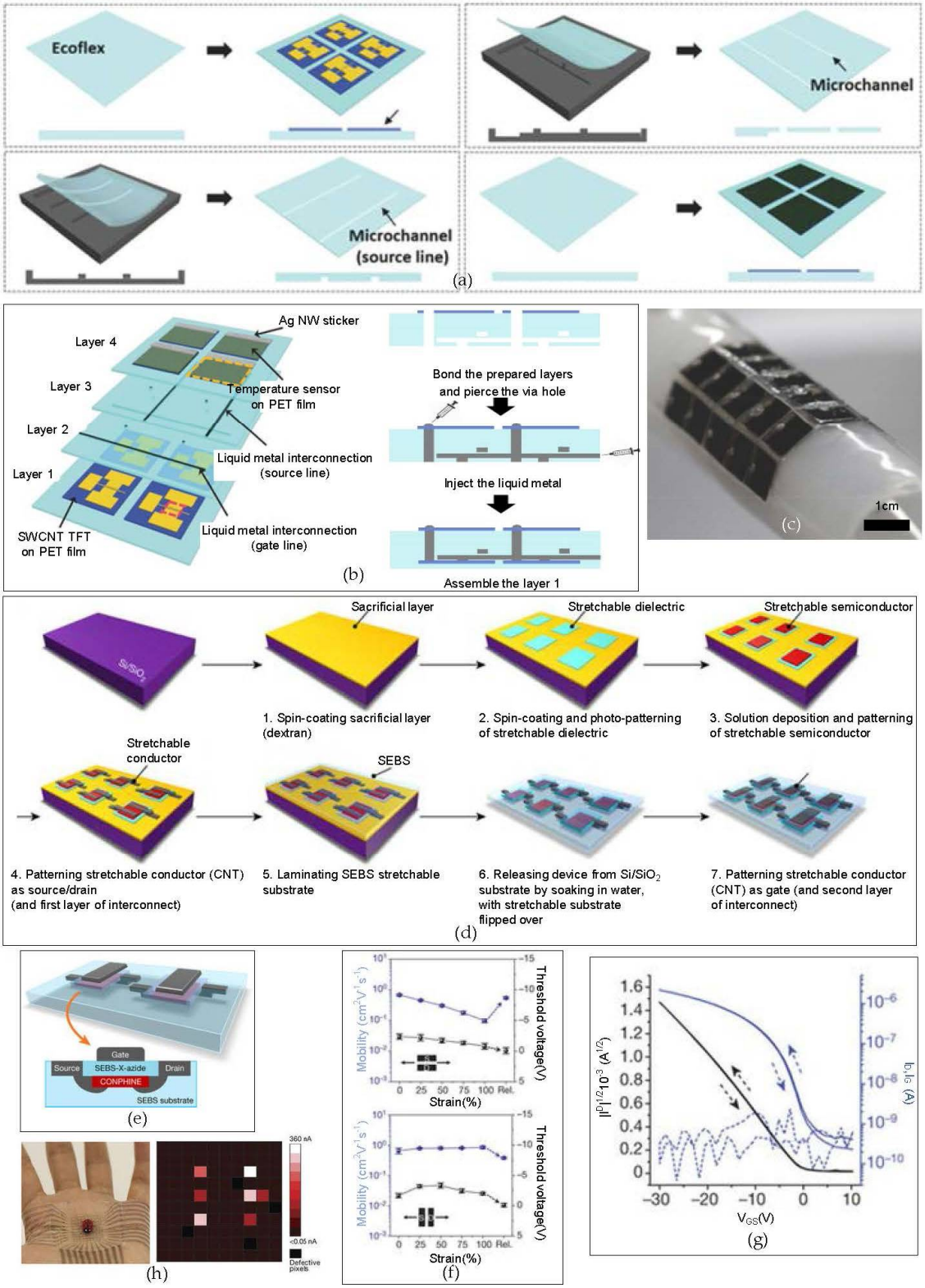

Figure 7. Stretchable temperature sensor arrays for electronic skin/Electronic skin based on stretchable transistor array (**a**) Schematic of fabricating the flexible and stretchable active matrix temperature sensor array; (**b**) Vertical schematic view of sensor(left) and injecting liquid metal for gate/source lines; (**c**) Optical image of bended sensor with radius of 14mm. Copyright 2016 Advanced Materials; (**d**) Schematic of fabrication process for arrays of flexible transistors; (**e**) Closer view of flexible transistor with high performance; (**f**) Mobility and threshold voltage change when applying strain from 0% to 100%; (**g**) I-V characteristic of fabricated transistors which has almost no hysteresis; (**h**) Stretchable arrays of transistors attached on the human palm with small artificial lady bug with 6 legs and corresponding result from the stretchable sensor. Copyright 2018 Nature.

4. Conclusions

This review summarizes some of the most recent developments in novel fabrication techniques of flexible and stretchable electronics. To minimize the defects created during the fabrication process, various nanoscale fabrications are required to fabricate flexible electronics. Since the required fabrication conditions for each technique are different as an example of temperature, choosing proper fabrication technique for each component of the flexible electronic device is needed. Various techniques introduced in this review show the great potentials of flexible electronics fabricated in nanoscale, which can be the cornerstone of future researches on fabricating biocompatible and implantable flexible electronics without any performance degradations.

Acknowledgments: K.K., Y.U.C., and K.J.Y. acknowledges support from National Research Foundation of Korea (Grant No. NRF-2017M1A2A2048904) and Yonsei University Future-leading Research Initiative of 2017 (RMS22017-22-00).

Author Contributions: K.K., Y.U.C., and K.J.Y. collected the data, contributed to the scientific discussions, and co-wrote the manuscript.

Conflicts of Interest: The authors declare no competing financial interests.

References

1. Gates, B.D.; Xu, Q.; Stewart, M.; Ryan, D.; Willson, C.G.; Whitesides, G.M. New approaches to nanofabrication: Molding, printing, and other techniques. Chemical reviews 2005, 105, 1171-1196.
2. Chen, Y.; Pepin, A. Nanofabrication: Conventional and nonconventional methods. Electrophoresis 2001, 22, 187-207.
3. Gates, B.D.; Xu, Q.; Love, J.C.; Wolfe, D.B.; Whitesides, G.M. Unconventional nanofabrication. Annu. Rev. Mater. Res. 2004, 34, 339-372.
4. Quake, S.R.; Scherer, A. From micro-to nanofabrication with soft materials. Science 2000, 290, 1536-1540.
5. Yang, L.; Akhatov, I.; Mahinfalah, M.; Jang, B.Z. Nano-fabrication: A review. Journal of the Chinese Institute of Engineers 2007, 30, 441-446.
6. Wang, X.; Lu, X.; Liu, B.; Chen, D.; Tong, Y.; Shen, G. Flexible energy-storage devices: Design consideration and recent progress. Advanced materials 2014, 26, 4763-4782.
7. Chen, H.; Cong, T.N.; Yang, W.; Tan, C.; Li, Y.; Ding, Y. Progress in electrical energy storage system: A critical review. Progress in Natural Science 2009, 19, 291-312.
8. Dong, L.; Xu, C.; Li, Y.; Huang, Z.-H.; Kang, F.; Yang, Q.-H.; Zhao, X. Flexible electrodes and supercapacitors for wearable energy storage: A review by category. Journal of Materials Chemistry A 2016, 4, 4659-4685.
9. Stoppa, M.; Chiolerio, A. Wearable electronics and smart textiles: A critical review. Sensors 2014, 14, 11957-11992.
10. Zeng, W.; Shu, L.; Li, Q.; Chen, S.; Wang, F.; Tao, X.M. Fiber-based wearable electronics: A review of materials, fabrication, devices, and applications. Advanced Materials 2014, 26, 5310-5336.

11. Tao, X. Wearable electronics and photonics. Elsevier: 2005.
12. Mukhopadhyay, S.C. Wearable sensors for human activity monitoring: A review. IEEE sensors journal 2015, 15, 1321-1330.
13. Chen, Y.; Au, J.; Kazlas, P.; Ritenour, A.; Gates, H.; McCreary, M. Electronic paper: Flexible active-matrix electronic ink display. Nature 2003, 423, 136.
14. Chang, P.-L.; Wu, C.-C.; Leu, H.-J. Investigation of technological trends in flexible display fabrication through patent analysis. Displays 2012, 33, 68-73.
15. Chung, I.-J.; Kang, I. Flexible display technology–opportunity and challenges to new business application. Molecular Crystals and Liquid Crystals 2009, 507, 1-17.
16. Biswas, A.; Bayer, I.S.; Biris, A.S.; Wang, T.; Dervishi, E.; Faupel, F. Advances in top–down and bottom–up surface nanofabrication: Techniques, applications & future prospects. Advances in colloid and interface science 2012, 170, 2-27.
17. Khanna, V.K. Top-down nanofabrication. In Integrated nanoelectronics, Springer: 2016; pp 381-396.
18. Mijatovic, D.; Eijkel, J.C.; van den Berg, A. Technologies for nanofluidic systems: Top-down vs. Bottom-up—a review. Lab on a Chip 2005, 5, 492-500.
19. Molnár, G.; Cobo, S.; Real, J.A.; Carcenac, F.; Daran, E.; Vieu, C.; Bousseksou, A. A combined top-down/bottom-up approach for the nanoscale patterning of spin-crossover coordination polymers. Advanced Materials 2007, 19, 2163-2167.
20. Cavallini, M.; Facchini, M.; Massi, M.; Biscarini, F. Bottom–up nanofabrication of materials for organic electronics. Synthetic metals 2004, 146, 283-286.
21. Khanna, V.K. Bottom-up nanofabrication. In Integrated nanoelectronics, Springer: 2016; pp 397-417.
22. Lu, W.; Lieber, C.M. Nanoelectronics from the bottom up. Nature materials 2007, 6, 841.
23. Levinson, H.J. Lithography process control. SPIE Optical Engineering Press Bellingham, WA: 1999.
24. Watt, F.; Bettiol, A.; Van Kan, J.; Teo, E.; Breese, M. Ion beam lithography and nanofabrication: A review. International Journal of Nanoscience 2005, 4, 269-286.
25. Bondur, J.A. Dry process technology (reactive ion etching). Journal of Vacuum Science and Technology 1976, 13, 1023-1029.
26. Jansen, H.; Gardeniers, H.; de Boer, M.; Elwenspoek, M.; Fluitman, J. A survey on the reactive ion etching of silicon in microtechnology. Journal of micromechanics and microengineering 1996, 6, 14.
27. Yih, P.; Saxena, V.; Steckl, A. A review of sic reactive ion etching in fluorinated plasmas. physica status solidi (b) 1997, 202, 605-642.
28. Zardetto, V.; Brown, T.M.; Reale, A.; Di Carlo, A. Substrates for flexible electronics: A practical investigation on the electrical, film flexibility, optical, temperature, and solvent resistance properties. Journal of Polymer Science Part B: Polymer Physics 2011, 49, 638-648.
29. Carlson, A.; Bowen, A.M.; Huang, Y.; Nuzzo, R.G.; Rogers, J.A. Transfer printing techniques for materials assembly and micro/nanodevice fabrication. Advanced Materials 2012, 24, 5284-5318.
30. Hines, D.; Ballarotto, V.; Williams, E.; Shao, Y.; Solin, S. Transfer printing methods for the fabrication of flexible organic electronics. Journal of applied physics 2007, 101, 024503.
31. Lee, C.H.; Kim, D.R.; Zheng, X. Fabricating nanowire devices on diverse substrates by simple transfer-printing methods. Proceedings of the National Academy of Sciences 2010, 107, 9950-9955.
32. Lee, C.H.; Kim, D.R.; Zheng, X. Transfer printing methods for flexible thin film solar cells: Basic concepts and working principles. Acs Nano 2014, 8, 8746-8756.
33. Sun, Y.; Rogers, J.A. Fabricating semiconductor nano/microwires and transfer printing ordered arrays of them onto plastic substrates. Nano Letters 2004, 4, 1953-1959.
34. Ji, S.; Liu, C.-C.; Liu, G.; Nealey, P.F. Molecular transfer printing using block copolymers. ACS nano 2009, 4, 599-609.
35. Loo, Y.-L.; Willett, R.L.; Baldwin, K.W.; Rogers, J.A. Interfacial chemistries for nanoscale transfer printing. Journal of the American Chemical Society 2002, 124, 7654-7655.
36. Meitl, M.A.; Zhu, Z.-T.; Kumar, V.; Lee, K.J.; Feng, X.; Huang, Y.Y.; Adesida, I.; Nuzzo, R.G.; Rogers, J.A. Transfer printing by kinetic control of adhesion to an elastomeric stamp. Nature materials 2006, 5, 33.
37. Espinha, A.; Dore, C.; Matricardi, C.; Alonso, M.I.; Goñi, A.R.; Mihi, A. Hydroxypropyl cellulose photonic architectures by soft nanoimprinting lithography. Nature Photonics 2018, 1.
38. Ishikawa, A.; Shffiata, T. Cellulosic chiral stationary phase under reversed-phase condition. Journal of Liquid Chromatography & Related Technologies 1993, 16, 859-878.

39. O'brien, T.; Crocker, L.; Thompson, R.; Thompson, K.; Toma, P.; Conlon, D.; Feibush, B.; Moeder, C.; Bicker, G.; Grinberg, N. Mechanistic aspects of chiral discrimination on modified cellulose. Analytical Chemistry 1997, 69, 1999-2007.
40. Revol, J.-F.; Godbout, L.; Dong, X.-M.; Gray, D.G.; Chanzy, H.; Maret, G. Chiral nematic suspensions of cellulose crystallites; phase separation and magnetic field orientation. Liquid Crystals 1994, 16, 127-134.
41. Shopsowitz, K.E.; Hamad, W.Y.; MacLachlan, M.J. Chiral nematic mesoporous carbon derived from nanocrystalline cellulose. Angewandte Chemie International Edition 2011, 50, 10991-10995.
42. Qin, D.; Xia, Y.; Whitesides, G.M. Soft lithography for micro-and nanoscale patterning. Nature protocols 2010, 5, 491.
43. Rogers, J.A.; Nuzzo, R.G. Recent progress in soft lithography. Materials today 2005, 8, 50-56.
44. Rolland, J.P.; Hagberg, E.C.; Denison, G.M.; Carter, K.R.; De Simone, J.M. High-resolution soft lithography: Enabling materials for nanotechnologies. Angewandte Chemie International Edition 2004, 43, 5796-5799.
45. Whitesides, G.M.; Ostuni, E.; Takayama, S.; Jiang, X.; Ingber, D.E. Soft lithography in biology and biochemistry. Annual review of biomedical engineering 2001, 3, 335-373.
46. Xia, Y.; Whitesides, G.M. Soft lithography. Annual review of materials science 1998, 28, 153-184.
47. Demeester, P.; Pollentier, I.; De Dobbelaere, P.; Brys, C.; Van Daele, P. Epitaxial lift-off and its applications. Semiconductor Science and Technology 1993, 8, 1124.
48. Liao, W.-S.; Cheunkar, S.; Cao, H.H.; Bednar, H.R.; Weiss, P.S.; Andrews, A.M. Subtractive patterning via chemical lift-off lithography. Science 2012, 337, 1517-1521.
49. Yu, X.; Wang, H.; Ning, X.; Sun, R.; Albadawi, H.; Salomao, M.; Silva, A.C.; Yu, Y.; Tian, L.; Koh, A. Needle-shaped ultrathin piezoelectric microsystem for guided tissue targeting via mechanical sensing. Nature Biomedical Engineering 2018, 2, 165.
50. Abramowitch, S.D.; Feola, A.; Jallah, Z.; Moalli, P.A. Tissue mechanics, animal models, and pelvic organ prolapse: A review. European Journal of Obstetrics and Gynecology and Reproductive Biology 2009, 144, S146-S158.
51. Cowin, S.C.; Doty, S.B. Tissue mechanics. Springer Science & Business Media: 2007.
52. Discher, D.E.; Janmey, P.; Wang, Y.-l. Tissue cells feel and respond to the stiffness of their substrate. Science 2005, 310, 1139-1143.
53. Hoyt, K.; Castaneda, B.; Zhang, M.; Nigwekar, P.; di Sant'Agnese, P.A.; Joseph, J.V.; Strang, J.; Rubens, D.J.; Parker, K.J. Tissue elasticity properties as biomarkers for prostate cancer. Cancer Biomarkers 2008, 4, 213-225.
54. Kenedi, R.; Gibson, T.; Evans, J.; Barbenel, J. Tissue mechanics. physics in Medicine & Biology 1975, 20, 699.
55. Bassett, C.A.L. Biologic significance of piezoelectricity. Calcified tissue research 1967, 1, 252-272.
56. Marino, A.A.; Becker, R.O.; Soderholm, S.C. Origin of the piezoelectric effect in bone. Calcified tissue research 1971, 8, 177-180.
57. Ribeiro, C.; Sencadas, V.; Correia, D.M.; Lanceros-Méndez, S. Piezoelectric polymers as biomaterials for tissue engineering applications. Colloids and Surfaces B: Biointerfaces 2015, 136, 46-55.
58. Shamos, M.H.; Lavine, L.S. Piezoelectricity as a fundamental property of biological tissues. Nature 1967, 213, 267.
59. Telega, J.J.; Wojnar, R. Piezoelectric effects in biological tissues. Journal of Theoretical and Applied mechanics 2002, 40, 723-759.
60. Arda, K.; Ciledag, N.; Aktas, E.; Arıbas, B.K.; Köse, K. Quantitative assessment of normal soft-tissue elasticity using shear-wave ultrasound elastography. American Journal of Roentgenology 2011, 197, 532-536.
61. Kruse, S.; Smith, J.; Lawrence, A.; Dresner, M.; Manduca, A.; Greenleaf, J.F.; Ehman, R.L. Tissue characterization using magnetic resonance elastography: Preliminary results. Physics in Medicine & Biology 2000, 45, 1579.
62. Manduca, A.; Oliphant, T.E.; Dresner, M.; Mahowald, J.; Kruse, S.A.; Amromin, E.; Felmlee, J.P.; Greenleaf, J.F.; Ehman, R.L. Magnetic resonance elastography: Non-invasive mapping of tissue elasticity. Medical image analysis 2001, 5, 237-254.
63. Ophir, J.; Cespedes, I.; Garra, B.; Ponnekanti, H.; Huang, Y.; Maklad, N. Elastography: Ultrasonic imaging of tissue strain and elastic modulus in vivo. European journal of ultrasound 1996, 3, 49-70.
64. Ophir, J.; Cespedes, I.; Ponnekanti, H.; Yazdi, Y.; Li, X. Elastography: A quantitative method for imaging the elasticity of biological tissues. Ultrasonic imaging 1991, 13, 111-134.

65. Gross, R.E.; Krack, P.; Rodriguez-Oroz, M.C.; Rezai, A.R.; Benabid, A.L. Electrophysiological mapping for the implantation of deep brain stimulators for parkinson's disease and tremor. Movement disorders 2006, 21.
66. Josephson, M.E. Clinical cardiac electrophysiology: Techniques and interpretations. Lippincott Williams & Wilkins: 2008.
67. Sigg, D.C.; Iaizzo, P.A.; Xiao, Y.-F.; He, B. Cardiac electrophysiology methods and models. Springer Science & Business Media: 2010.
68. Viventi, J.; Kim, D.-H.; Moss, J.D.; Kim, Y.-S.; Blanco, J.A.; Annetta, N.; Hicks, A.; Xiao, J.; Huang, Y.; Callans, D.J. A conformal, bio-interfaced class of silicon electronics for mapping cardiac electrophysiology. Science translational medicine 2010, 2, 24ra22-24ra22.
69. Merrill, D.R.; Bikson, M.; Jefferys, J.G. Electrical stimulation of excitable tissue: Design of efficacious and safe protocols. Journal of neuroscience methods 2005, 141, 171-198.
70. Peckham, P.H.; Knutson, J.S. Functional electrical stimulation for neuromuscular applications. Annu. Rev. Biomed. Eng. 2005, 7, 327-360.
71. Tandon, N.; Cannizzaro, C.; Chao, P.-H.G.; Maidhof, R.; Marsano, A.; Au, H.T.H.; Radisic, M.; Vunjak-Novakovic, G. Electrical stimulation systems for cardiac tissue engineering. Nature protocols 2009, 4, 155.
72. Aravanis, A.M.; Wang, L.-P.; Zhang, F.; Meltzer, L.A.; Mogri, M.Z.; Schneider, M.B.; Deisseroth, K. An optical neural interface: In vivo control of rodent motor cortex with integrated fiberoptic and optogenetic technology. Journal of neural engineering 2007, 4, S143.
73. Duke, A.R.; Lu, H.; Jenkins, M.W.; Chiel, H.J.; Jansen, E.D. Spatial and temporal variability in response to hybrid electro-optical stimulation. Journal of neural engineering 2012, 9, 036003.
74. Richter, C.P.; Matic, A.I.; Wells, J.D.; Jansen, E.D.; Walsh, J.T. Neural stimulation with optical radiation. Laser & photonics reviews 2011, 5, 68-80.
75. Wells, J.; Kao, C.; Konrad, P.; Milner, T.; Kim, J.; Mahadevan-Jansen, A.; Jansen, E.D. Biophysical mechanisms of transient optical stimulation of peripheral nerve. Biophysical journal 2007, 93, 2567-2580.
76. Park, S.I.; Brenner, D.S.; Shin, G.; Morgan, C.D.; Copits, B.A.; Chung, H.U.; Pullen, M.Y.; Noh, K.N.; Davidson, S.; Oh, S.J. Soft, stretchable, fully implantable miniaturized optoelectronic systems for wireless optogenetics. Nature biotechnology 2015, 33, 1280.
77. Robinson, R. Optogenetics sheds light on brain circuits. Is therapy next? Neurology Today 2010, 10, 16-17.
78. Williams, J.C.; Denison, T. From optogenetic technologies to neuromodulation therapies. Science translational medicine 2013, 5, 177ps176-177ps176.
79. Feiner, R.; Engel, L.; Fleischer, S.; Malki, M.; Gal, I.; Shapira, A.; Shacham-Diamand, Y.; Dvir, T. Engineered hybrid cardiac patches with multifunctional electronics for online monitoring and regulation of tissue function. Nature materials 2016, 15, 679.
80. Yu, K.J.; Kuzum, D.; Hwang, S.-W.; Kim, B.H.; Juul, H.; Kim, N.H.; Won, S.M.; Chiang, K.; Trumpis, M.; Richardson, A.G. Bioresorbable silicon electronics for transient spatiotemporal mapping of electrical activity from the cerebral cortex. Nature materials 2016, 15, 782.
81. Sun, Y.; Rogers, J.A. Semiconductor nanomaterials for flexible technologies. Elsevier/William Andrew: Amsterdam ;London :, 2010.
82. Lee, T.; Lee, W.; Kim, S.W.; Kim, J.J.; Kim, B.S. Flexible textile strain wireless sensor functionalized with hybrid carbon nanomaterials supported zno nanowires with controlled aspect ratio. Advanced Functional Materials 2016, 26, 6206-6214.
83. Gao, Q.; Dubrovskii, V.G.; Caroff, P.; Wong-Leung, J.; Li, L.; Guo, Y.; Fu, L.; Tan, H.H.; Jagadish, C. Simultaneous selective-area and vapor–liquid–solid growth of inp nanowire arrays. Nano Letters 2016, 16, 4361-4367.
84. Lee, W.C.; Kim, K.; Park, J.; Koo, J.; Jeong, H.Y.; Lee, H.; Weitz, D.A.; Zettl, A.; Takeuchi, S. Graphene-templated directional growth of an inorganic nanowire. Nature Nanotechnology 2015, 10, 423.
85. Holmes, J.D.; Johnston, K.P.; Doty, R.C.; Korgel, B.A. Control of thickness and orientation of solution-grown silicon nanowires. Science 2000, 287, 1471-1473.
86. Persson, A.I.; Larsson, M.W.; Stenström, S.; Ohlsson, B.J.; Samuelson, L.; Wallenberg, L.R. Solid-phase diffusion mechanism for gaas nanowire growth. Nature Materials 2004, 3, 677.
87. Zhu, B.; Niu, Z.; Wang, H.; Leow, W.R.; Wang, H.; Li, Y.; Zheng, L.; Wei, J.; Huo, F.; Chen, X. Microstructured graphene arrays for highly sensitive flexible tactile sensors. Small 2014, 10, 3625-3631.

88. Li, X.; Yang, T.; Yang, Y.; Zhu, J.; Li, L.; Alam, F.E.; Li, X.; Wang, K.; Cheng, H.; Lin, C.T., et al. Large-area ultrathin graphene films by single-step marangoni self-assembly for highly sensitive strain sensing application. Advanced Functional Materials 2016, 26, 1322-1329.
89. Gong, S.; Zhao, Y.; Yap, L.W.; Shi, Q.; Wang, Y.; Bay, J.A.P.B.; Lai, D.T.H.; Uddin, H.; Cheng, W. Fabrication of highly transparent and flexible nanomesh electrode via self-assembly of ultrathin gold nanowires. Advanced Electronic Materials 2016, 2, 1600121.
90. Hong, S.Y.; Lee, Y.H.; Park, H.; Jin, S.W.; Jeong, Y.R.; Yun, J.; You, I.; Zi, G.; Ha, J.S. Stretchable active matrix temperature sensor array of polyaniline nanofibers for electronic skin. Advanced Materials 2016, 28, 930-935.
91. Rhyee, J.S.; Kwon, J.; Dak, P.; Kim, J.H.; Kim, S.M.; Park, J.; Hong, Y.K.; Song, W.G.; Omkaram, I.; Alam, M.A., et al. High-mobility transistors based on large-area and highly crystalline cvd-grown mose2 films on insulating substrates. Advanced Materials 2016, 28, 2316-2321.
92. Dai, X.; Messanvi, A.; Zhang, H.; Durand, C.; Eymery, J.; Bougerol, C.; Julien, F.H.; Tchernycheva, M. Flexible light-emitting diodes based on vertical nitride nanowires. Nano Letters 2015, 15, 6958-6964.
93. Lee, Y.H.; Zhang, X.Q.; Zhang, W.; Chang, M.T.; Lin, C.T.; Chang, K.D.; Yu, Y.C.; Wang, J.T.W.; Chang, C.S.; Li, L.J., et al. Synthesis of large-area mos2 atomic layers with chemical vapor deposition. Advanced Materials 2012, 24, 2320-2325.
94. Zhan, Y.; Liu, Z.; Najmaei, S.; Ajayan, P.M.; Lou, J. Large-area vapor-phase growth and characterization of mos2 atomic layers on a sio2 substrate. Small 2012, 8, 966-971.
95. van der Zande, A.M.; Huang, P.Y.; Chenet, D.A.; Berkelbach, T.C.; You, Y.; Lee, G.-H.; Heinz, T.F.; Reichman, D.R.; Muller, D.A.; Hone, J.C. Grains and grain boundaries in highly crystalline monolayer molybdenum disulphide. Nature Materials 2013, 12, 554.
96. Liu, K.-K.; Zhang, W.; Lee, Y.-H.; Lin, Y.-C.; Chang, M.-T.; Su, C.-Y.; Chang, C.-S.; Li, H.; Shi, Y.; Zhang, H., et al. Growth of large-area and highly crystalline mos2 thin layers on insulating substrates. Nano Letters 2012, 12, 1538-1544.
97. Meng, Y.; Gu, D.; Zhang, F.; Shi, Y.; Cheng, L.; Feng, D.; Wu, Z.; Chen, Z.; Wan, Y.; Stein, A., et al. A family of highly ordered mesoporous polymer resin and carbon structures from organic–organic self-assembly. Chemistry of Materials 2006, 18, 4447-4464.
98. Yu, D.; Dai, L. Self-assembled graphene/carbon nanotube hybrid films for supercapacitors. The Journal of Physical Chemistry Letters 2010, 1, 467-470.
99. Engel, M.; Small, J.P.; Steiner, M.; Freitag, M.; Green, A.A.; Hersam, M.C.; Avouris, P. Thin film nanotube transistors based on self-assembled, aligned, semiconducting carbon nanotube arrays. ACS Nano 2008, 2, 2445-2452.
100. Margenau, H. Van der waals forces. Reviews of Modern Physics 1939, 11, 1-35.
101. Zaremba, E.; Kohn, W. Van der waals interaction between an atom and a solid surface. Physical Review B 1976, 13, 2270-2285.
102. Morokuma, K. Molecular orbital studies of hydrogen bonds. Iii. C=o···h–o hydrogen bond in h2co···h2o and h2co···2h2o. The Journal of Chemical Physics 1971, 55, 1236-1244.
103. Janiak, C. A critical account on [small pi]-[small pi] stacking in metal complexes with aromatic nitrogen-containing ligands. Journal of the Chemical Society, Dalton Transactions 2000, 3885-3896.
104. Grimme, S. Do special noncovalent π–π stacking interactions really exist? Angewandte Chemie International Edition 2008, 47, 3430-3434.
105. Wu, H.; Kong, D.; Ruan, Z.; Hsu, P.-C.; Wang, S.; Yu, Z.; Carney, T.J.; Hu, L.; Fan, S.; Cui, Y. A transparent electrode based on a metal nanotrough network. Nature Nanotechnology 2013, 8, 421.
106. Kim, S.; Kwon, H.J.; Lee, S.; Shim, H.; Chun, Y.; Choi, W.; Kwack, J.; Han, D.; Song, M.; Kim, S., et al. Low-power flexible organic light-emitting diode display device. Advanced Materials 2011, 23, 3511-3516.
107. Zhou, L.; Wanga, A.; Wu, S.-C.; Sun, J.; Park, S.; Jackson, T.N. All-organic active matrix flexible display. Applied Physics Letters 2006, 88, 083502.
108. Yagi, I.; Hirai, N.; Miyamoto, Y.; Noda, M.; Imaoka, A.; Yoneya, N.; Nomoto, K.; Kasahara, J.; Yumoto, A.; Urabe, T. A flexible full-color amoled display driven by otfts. Journal of the Society for Information Display 2008, 16, 15-20.
109. Sirringhaus, H.; Tessler, N.; Friend, R.H. Integrated optoelectronic devices based on conjugated polymers. Science 1998, 280, 1741-1744.

110. Tan, Z.; Xu, J.; Zhang, C.; Zhu, T.; Zhang, F.; Hedrick, B.; Pickering, S.; Wu, J.; Su, H.; Gao, S., et al. Colloidal nanocrystal-based light-emitting diodes fabricated on plastic toward flexible quantum dot optoelectronics. Journal of Applied Physics 2009, 105, 034312.
111. Shahi, S. Flexible optoelectronics. Nature Photonics 2010, 4, 506.
112. Choi, M.K.; Yang, J.; Hyeon, T.; Kim, D.-H. Flexible quantum dot light-emitting diodes for next-generation displays. npj Flexible Electronics 2018, 2, 10.
113. Yao, S.; Zhu, Y. Nanomaterial-enabled stretchable conductors: Strategies, materials and devices. Advanced Materials 2015, 27, 1480-1511.
114. Espinosa, H.D.; Bernal, R.A.; Minary-Jolandan, M. A review of mechanical and electromechanical properties of piezoelectric nanowires. Advanced Materials 2012, 24, 4656-4675.
115. Wang, Y.; Wang, F.; He, J. Controlled fabrication and photocatalytic properties of a three-dimensional zno nanowire/reduced graphene oxide/cds heterostructure on carbon cloth. Nanoscale 2013, 5, 11291-11297.
116. Xu, J.; Wang, K.; Zu, S.-Z.; Han, B.-H.; Wei, Z. Hierarchical nanocomposites of polyaniline nanowire arrays on graphene oxide sheets with synergistic effect for energy storage. ACS Nano 2010, 4, 5019-5026.
117. Novoselov, K.S.; Geim, A.K.; Morozov, S.V.; Jiang, D.; Zhang, Y.; Dubonos, S.V.; Grigorieva, I.V.; Firsov, A.A. Electric field effect in atomically thin carbon films. Science 2004, 306, 666-669.
118. Geim, A.K.; Novoselov, K.S. The rise of graphene. Nature Materials 2007, 6, 183.
119. Lee, C.; Wei, X.; Kysar, J.W.; Hone, J. Measurement of the elastic properties and intrinsic strength of monolayer graphene. Science 2008, 321, 385-388.
120. Nair, R.R.; Blake, P.; Grigorenko, A.N.; Novoselov, K.S.; Booth, T.J.; Stauber, T.; Peres, N.M.R.; Geim, A.K. Fine structure constant defines visual transparency of graphene. Science 2008, 320, 1308-1308.
121. Kovtyukhova, N.I.; Ollivier, P.J.; Martin, B.R.; Mallouk, T.E.; Chizhik, S.A.; Buzaneva, E.V.; Gorchinskiy, A.D. Layer-by-layer assembly of ultrathin composite films from micron-sized graphite oxide sheets and polycations. Chemistry of Materials 1999, 11, 771-778.
122. Zhang, M.; Gong, K.; Zhang, H.; Mao, L. Layer-by-layer assembled carbon nanotubes for selective determination of dopamine in the presence of ascorbic acid. Biosensors and Bioelectronics 2005, 20, 1270-1276.
123. Yang, M.; Yang, Y.; Yang, H.; Shen, G.; Yu, R. Layer-by-layer self-assembled multilayer films of carbon nanotubes and platinum nanoparticles with polyelectrolyte for the fabrication of biosensors. Biomaterials 2006, 27, 246-255.
124. Lee, S.W.; Kim, B.-S.; Chen, S.; Shao-Horn, Y.; Hammond, P.T. Layer-by-layer assembly of all carbon nanotube ultrathin films for electrochemical applications. Journal of the American Chemical Society 2009, 131, 671-679.
125. Eda, G.; Fanchini, G.; Chhowalla, M. Large-area ultrathin films of reduced graphene oxide as a transparent and flexible electronic material. Nature Nanotechnology 2008, 3, 270.
126. Compton, O.C.; Nguyen, S.T. Graphene oxide, highly reduced graphene oxide, and graphene: Versatile building blocks for carbon-based materials. Small 2010, 6, 711-723.
127. Maillard, M.; Motte, L.; Ngo, A.T.; Pileni, M.P. Rings and hexagons made of nanocrystals: A marangoni effect. The Journal of Physical Chemistry B 2000, 104, 11871-11877.
128. Sternling, C.V.; Scriven, L.E. Interfacial turbulence: Hydrodynamic instability and the marangoni effect. AIChE Journal 1959, 5, 514-523.
129. Fanton, X.; Cazabat, A.M. Spreading and instabilities induced by a solutal marangoni effect. Langmuir 1998, 14, 2554-2561.
130. Hu, N.; Karube, Y.; Yan, C.; Masuda, Z.; Fukunaga, H. Tunneling effect in a polymer/carbon nanotube nanocomposite strain sensor. Acta Materialia 2008, 56, 2929-2936.
131. Wang, S.; Xu, J.; Wang, W.; Wang, G.-J.N.; Rastak, R.; Molina-Lopez, F.; Chung, J.W.; Niu, S.; Feig, V.R.; Lopez, J., et al. Skin electronics from scalable fabrication of an intrinsically stretchable transistor array. Nature 2018, 555, 83.